

Granulation Rate Processes in the Kneading Elements of a Twin Screw Granulator

A. S. El Hagrasy

School of Chemical Engineering, Purdue University, West Lafayette, IN 47907

J. D. Litster

School of Chemical Engineering, Purdue University, West Lafayette, IN 47907

Dept. of Industrial and Physical Pharmacy, Purdue University, West Lafayette, IN 47907

DOI 10.1002/aic.14180

Published online August 28, 2013 in Wiley Online Library (wileyonlinelibrary.com)

To characterize the granulation rate processes in the kneading section of the twin screw granulator, separate experiments were conducted using exclusively conveying elements as the baseline in addition to different configurations of kneading elements. The configuration parameters examined were the length of the kneading section, the advance angle, and the angle direction. Granule size, shape and liquid distribution were measured. Two main rate processes were observed (1) breakage and layering, and (2) Shear elongation and layering. Breakage was dominant in the 90° configuration while shear elongation dominated in the 30° reverse configurations, with other configurations giving some combination of the two rate processes. The distinct three-dimensional (3-D) shape characteristics of granules obtained from each configuration were crucial in elucidating the dominant granulation rate process in each case. The proposed granulation mechanisms explain the events leading to particular granule attributes, but more importantly provide insight into future optimization of twin screw granulation process. © 2013 American Institute of Chemical Engineers AIChE J, 59: 4100–4115, 2013

Keywords: liquid distribution, granule growth, granule shape, granulation rate processes, screw element configuration, regime-separated granulation, mechanistic study

Introduction

Wet granulation is the process of agglomerating particles with the aid of a granulating liquid and the application of agitation force to form granules.¹ Wet granulation is widely implemented in industries that manufacture particulate products to improve powder properties, thereby facilitating handling and downstream processing. Although continuous wet granulation is common practice in most industry sectors, wet granulation of pharmaceutical formulations has traditionally been a batch process.^{2–4} The prevalence of batch processing can be attributed in part to the relatively small volume production of pharmaceuticals compared to other industries such as food and chemicals. In addition, pharmaceutical products are subject to frequent product change and unique regulatory standards that made batch processing of pharmaceuticals more amenable than continuous manufacturing. However, changes in the regulatory environment combined with a need to reduce costs and improve process control have initiated a paradigm shift within the pharmaceutical industry toward continuous processing.

Among the different granulator designs available for continuous processing, the twin screw granulator (TSG) provides the optimum throughput needed for pharmaceutical manufac-

turing combined with the advantages of a continuous operating mode.⁵ The modular design of the equipment gives it additional versatility in terms of a multitude of available screw elements that can modify granule properties as well as the ease with which the location of the liquid and powder feed ports can be varied along the length of the equipment, thereby allowing for different residence times.^{6–10} The equipment has also demonstrated robustness toward variation in formulation properties, which is critical for maintaining product quality against unexpected changes in raw material attributes.¹¹

Recent studies by Dhenge and coworkers on mechanistic understanding of the twin screw granulation process and the identification of specific granulation mechanisms occurring in different compartments along the length of the granulator were reported in the literature.^{12–14} In one study, the authors examined the granule formation mechanism in the conveying section and the evolution of granule physical properties as they passed through additional compartments along the length of the granulator such as one or more kneading blocks and conveying sections.¹² Throughout this work, the configuration of the kneading block was maintained constant in terms of the number of kneading elements used, their offset angle and the angle direction. The authors identified nucleation by immersion as the primary mechanism for granule formation in the conveying section. In subsequent kneading and conveying sections, granules were subjected to a series of consolidation, coalescence and breakage events before exiting the granulator.

Correspondence concerning this article should be addressed to J. D. Litster at jlitster@purdue.edu.

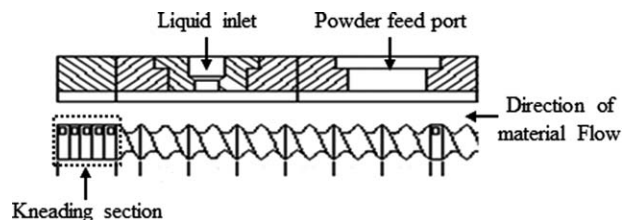


Figure 1. Abbreviated sample screw configuration illustrating the operational zone of the granulator with five kneading elements.

The unique design of the TSG, with well-defined regions for the different granulation rate processes, renders it a regime-separated granulator. Being a “regime-separated” process as such, one would expect better control over granule properties as opposed to conventional granulation equipment in which granulation rate processes occur simultaneously.¹⁵ However, several studies on twin-screw granulation reported a broad granule size distribution, with the presence of fines and lumps.^{5–8,11,16,17} A broad size distribution can have serious implications on the uniformity of granule drying as well as powder segregation during downstream processing; both of which are undesirable from an industrial perspective.

The study by El Hagrasy et al. identified the inadequacy of the kneading elements (KE) in distributing the granulating liquid as a potential cause for the broad granule-size distribution observed.¹¹ In a recent study, Dhenge et al. examined the effect of granulating liquid viscosity on the properties of granules produced from the conveying section only.¹⁴ The authors reported that the low shear imparted by the conveying elements was less effective in distributing the more viscous granulating liquid compared to another of lower viscosity. The liquid distribution attributes in both studies were inferred from characterizing granule physical properties, such as size and strength. Binder distribution was quantitatively measured using different analytical techniques in other types of batch granulators and correlated with the span of the granule size distribution.^{18–22} However, there is no direct quantitative information available on liquid distribution inside a TSG. Besides size information, other attributes such as the liquid distribution, porosity and the homogeneity of formulation components are essential for mechanistic understanding of a wet granulation process and accurate model development that can be implemented for process scale-up, optimization and control.²³

In this work, we provide a detailed report on the effect of individual screw elements on granule physical properties and liquid distribution. The effect of kneading element length and configuration on granule size, liquid and shape distribution is studied and compared to baseline results for a short conveying element section only. A combination of granulation rate processes for different configurations is proposed which explains these results and sets up the framework for future quantitative model development.

Experimental

Mechanistic studies

A model placebo formulation composed of α -lactose monohydrate (Pharmatose 200M, 73.5%), microcrystalline cellulose (Avicel PH101, 20%), hydroxypropylmethylcellulose (Hypromellose, 5%) and croscarmellose sodium (Ac-Di-Sol, 1.5%) was used in this work. The granulation experiments were carried out in a EuroLab 16 mm TSG, 25:1 L:D

(Thermo Fisher Scientific, Karlsruhe, Germany) using individual screw types as will be described in the next section. The powder feed rate was maintained at 4 kg/h using a gravimetric powder feeder (Brabender Flexwall® Feeder, Brabender-Technologie, Germany). The liquid feed rate was varied to allow increasing the L/S ratio between 0.15 and 0.35 at 0.05 increments. The granulating liquid used was composed of 0.1% (w/w) nigrosin dye in distilled water. A Masterflex® peristaltic pump (Cole Parmer, Vernon Hills, IL) was used to feed the granulating liquid to the granulator.

Screw configurations

In each screw characterization experiment, the screw section of interest was positioned in the last zone at the front end of the granulator and right after the liquid feed port. Figure 1 illustrates an abbreviated screw configuration of the operational zones in the TSG with five kneading elements as an example. The same setup was used for all other kneading block configurations. For experiments carried out in the conveying section only, conveying elements (CE) were used in place of the kneading elements (KE). Using the screw configuration in this manner minimized the interference from other screw elements on granule properties.

The functional role of individual screw elements was examined according to the screw configurations summarized in Table 1. At each L/S ratio, the granulation experiments were carried out using a short section of CE for liquid addition followed by a different number of KE: 3, 5 and 7, at 30°, 60° and 90° advance angles. The 30° and 60° angle configurations were used in both the forward (F) and the reverse (R) direction, whereas the 90° angle is considered neutral since it has only one angle direction. In a separate set of experiments, CE were used in the absence of KE to understand the evolution of granule properties as the material is transferred from the conveying section to the kneading section inside a TSG.

The isometric drawings in Figure 2 display the 3-D geometry of the barrel with 7 KE in the 30°F, 30°R, 60°F, 60°R and 90° angle configurations. The elements in each configuration have the same starting position, which is at the intersection of the first pair of adjacent KE’s tips in the middle channel from the driver end of the equipment. The F and R angle directions refer to the rotational direction of KE tips with respect to the flight of the preceding CE. The offset angle of the KE is considered to be in the forward direction if their outer lobes rotate in the same direction as the flights from the feeding screws and *vice versa* for the reverse direction. Figure 3A and 3B display a front view of the forward and reverse angle directions of KE at 60° angle configuration, respectively.

The gap volume indicates the space in the middle channel between the tips of each pair of KE, which changes depending on their orientation. For the 30° angle configuration, the KE are closely staged against the barrel wall as seen in Figure 2A and 2B, leaving a gap in the middle channel where

Table 1. Screw Configurations

Screw Type	Number	Advance Angle	Angle Direction
Conveying	—	—	—
	3, 5 and 7	30° 60°	Forward Reverse
KE	3, 5 and 7	30° 60°	Forward Reverse
	3, 5 and 7	90°	—

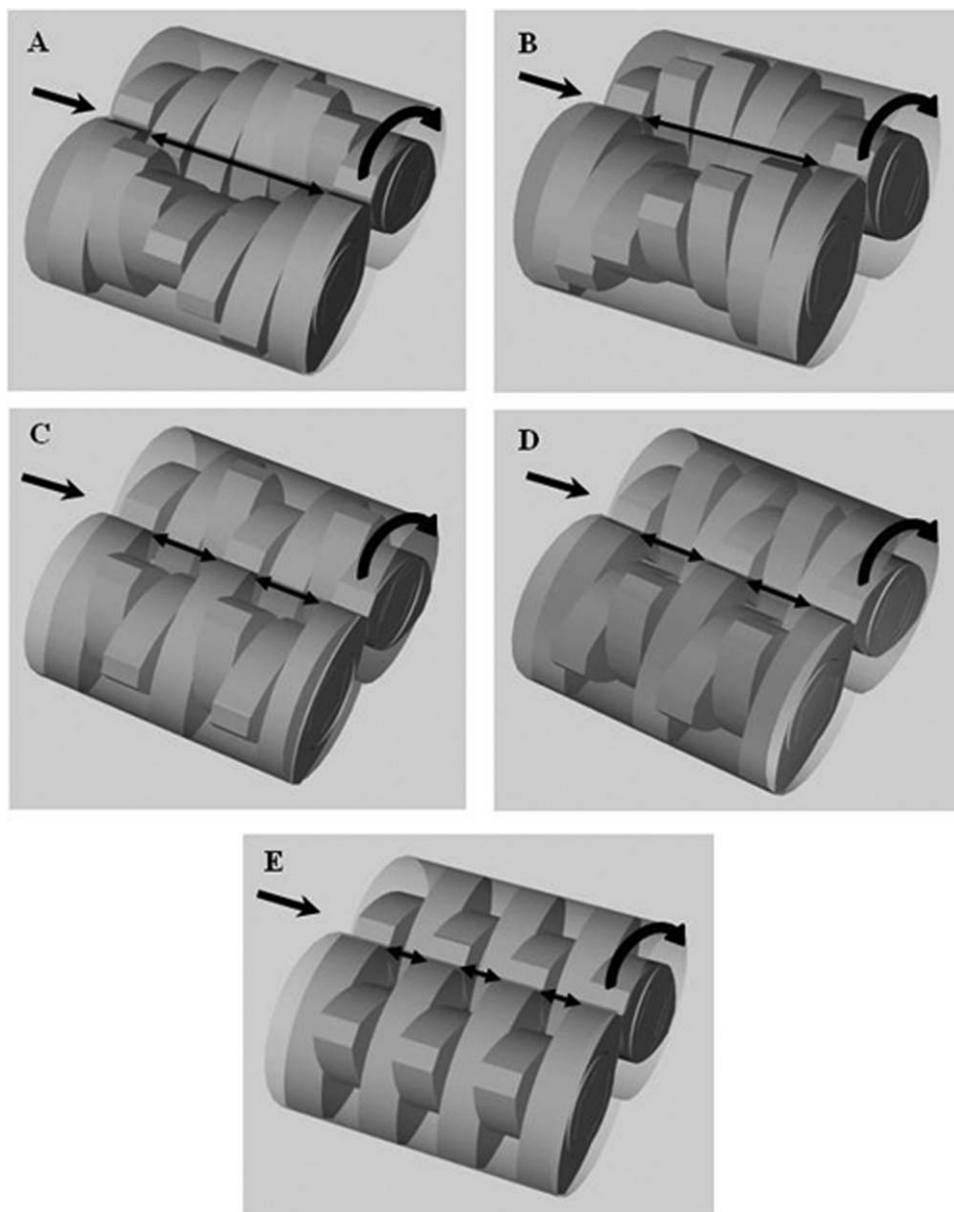


Figure 2. Configurations of kneading section using 7 KE at (A) 30°F, (B) 30°R, (C) 60°F, (D) 60°R and (E) 90°.

The curved arrow indicates the direction of rotation of the shafts and the straight arrow depicts the direction of material flow from the CE into the kneading section. The middle channel divergence length illustrated by the double-headed arrow is 1.25D for (A) and (B), 0.5D for (C) and (D) and 0.25D for (E).

the two barrels join. The divergence in the middle channel in this case is 1.25D long, i.e., there are 5 KE each 0.25D in thickness before the next pair of KE cross the middle channel again. As the offset angle is rotated to 60°, the gap in the middle channel decreases to be 0.5D in axial length before the KE tips reintersect (Figure 2C and 2D). In contrast, the middle channel is crossed by the tips of the adjacent pair of KE every 0.25D for the 90°, configuration (Figure 2E).

Granule characterization. The granules from all experiments were air-dried at ambient conditions for 48 h and split using a spinning riffler (Gilson Co., Inc., Lewis Center, OH) to ensure unbiased sampling for the subsequent granule characterization work.

Granule size distribution. Sieve analysis was used for measuring the size distribution of granules as described pre-

viously.¹¹ In brief, sieves following a $\sqrt{2}$ series ranging from 63 μm to 8 mm were used. All granule size distribution data was plotted as the normalized mass frequency of the logarithm of particle size according to the following equation²⁴

$$f(\ln x) = y_i / \ln(x_i / x_{i-1}) \quad (1)$$

where, y_i is the mass fraction in size interval i and x_i is the midpoint of the size interval i .

Analysis of Liquid Distribution. A water-soluble nigrosin dye (Sigma Aldrich Corp., St. Louis, MO), was used as a tracer in the granulating liquid to allow the determination of liquid distribution in different size fractions after drying the granules similar to the method reported by Smirani-Khayati et al.²¹ A UV/Vis spectroscopic method was used to analyze the amount of nigrosin dye in each sieved granule fraction. Three granule samples from each size fraction were analyzed. However, granule fractions that represented <1% of

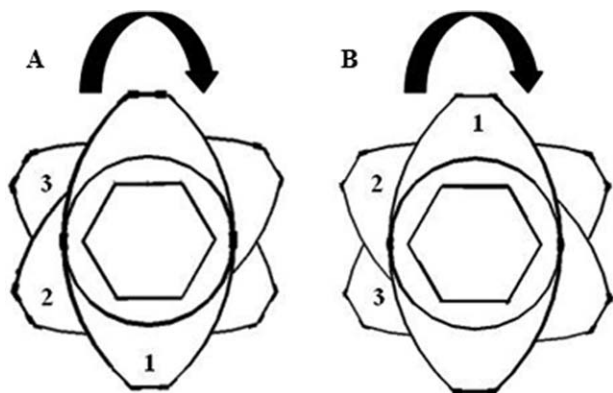


Figure 3. Two-dimensional (2-D) front view of the screw configuration for 3KE60° in the (A) forward angle direction, and (B) reverse angle direction.

The incremental order of KE shows the elements from front to back. The curved arrow indicates the direction of rotation of the shafts.

the total weight of the sieved granules were not analyzed for their dye content.

Each granule sample was mixed with 5 mL of distilled water in a glass vial and sonicated for 1 h. The suspension was then poured into 15 mL centrifuge tubes. Each glass vial was rinsed with another 5 mL of distilled water. The samples were centrifuged for 7 min at 11,000 rpm using an Eppendorf Centrifuge 5804, followed by withdrawing 5 mL of the supernatant. The absorbance of the dye solution was measured using a UV/Vis spectrophotometer (Cary UV Vis 300, Agilent, Wilmington, DE) at $\lambda_{\text{max}} = 574$ nm. The concentration of the dye in the sample was determined using a quantitative UV calibration in the range from 0.005 to 0.05 mg/mL ($R^2 = 0.9999$). We assume liquid distribution corresponds exactly to the dye distribution throughout the text hereafter.

Three-Dimensional (3-D) Shape Characterization. The shape of granules from selected experiments was characterized by imaging using a Nikon SMZ-1500 stereoscopic zoom microscope. A prism was used to capture the height of the granule in the same image as the projected area view according to the method described by Emady et al.²⁵ For

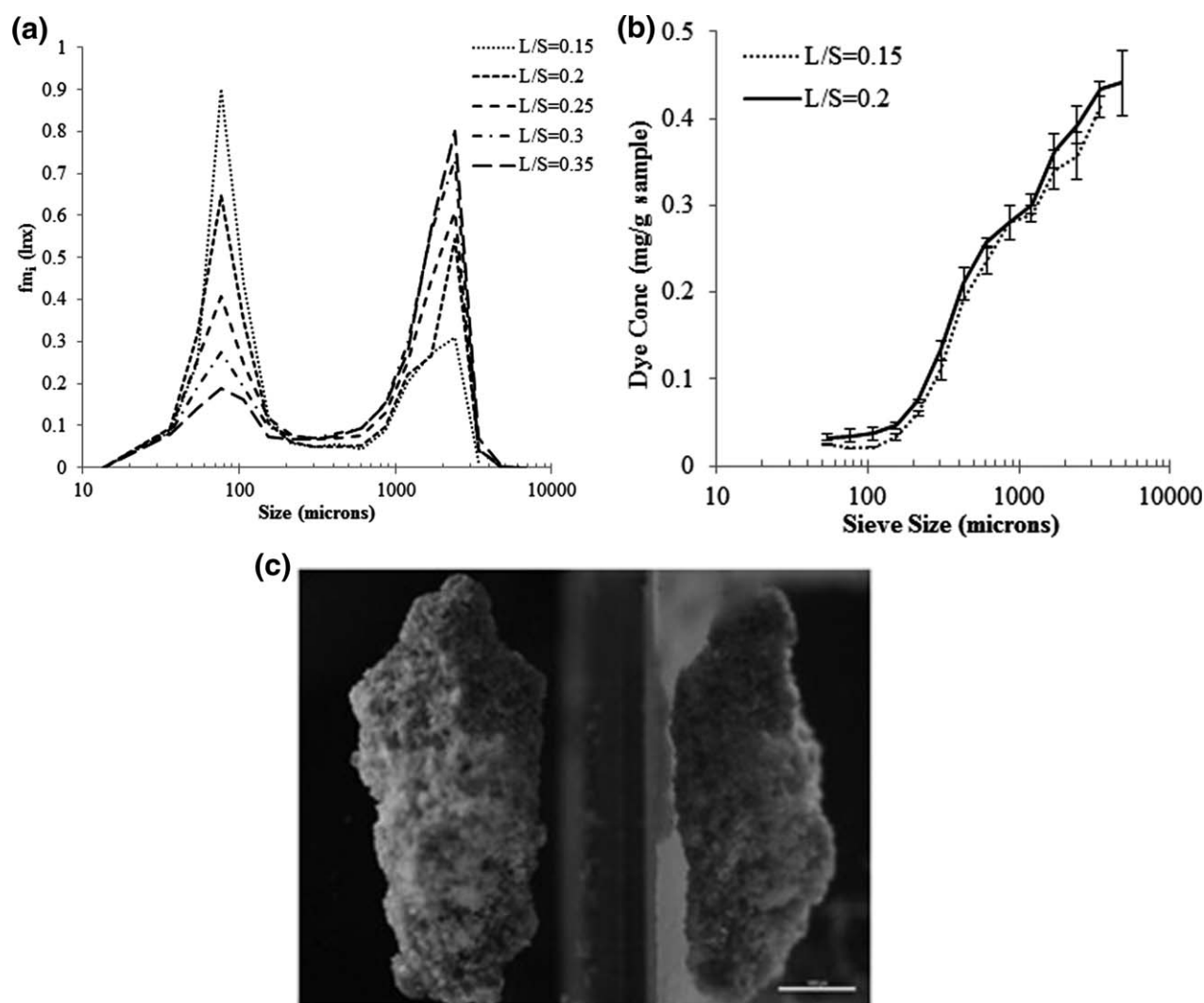


Figure 4. (A) The change in size distribution of granules from the conveying section at different L/S ratios; B. the concentration of nigrosin dye in the different size fractions of granules from the conveying section; the error bar at each data point is the standard deviation of three measurements; C. micrographs of top (left) and side (right) view of a representative granule from the conveying section.

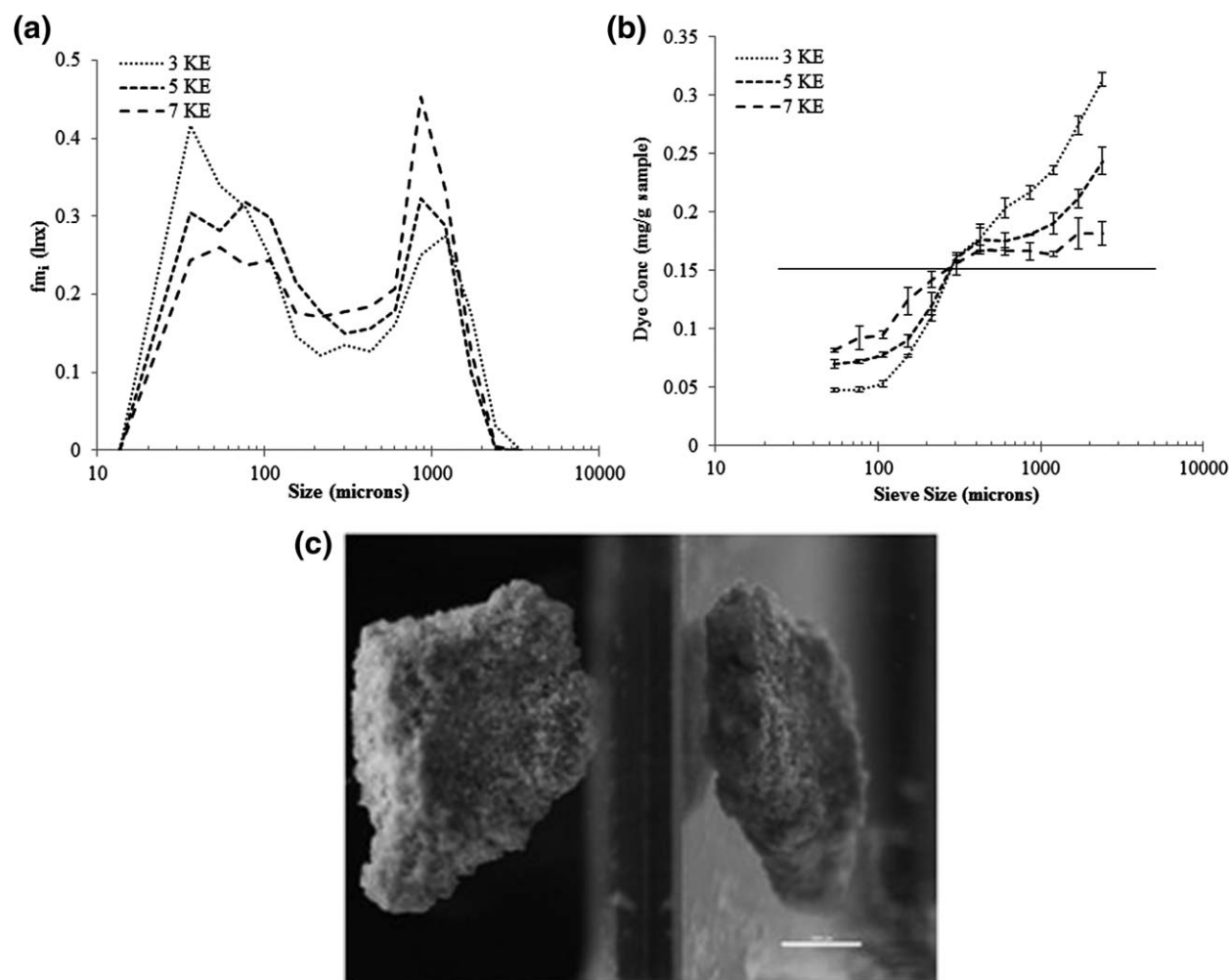


Figure 5. A. The frequency granule size distribution using 3 KE, 5 KE and 7 KE at 30°F angle configuration; B. dye distribution in granule size fractions using 3 KE, 5 KE and 7 KE at 30°F angle configuration; the horizontal solid line is the nominal dye concentration; the error bar at each data point is the standard deviation of three measurements; C. micrographs of top (left) and side (right) view of a representative granule from the 30°F kneading block configuration using 3 KE.

each experiment, images of 60 granules in the size range from 2–2.8 mm were collected and analyzed using Adobe Photoshop CS4 with the Fovea Pro 4.0 plug-in. The vertical aspect ratio (VAR) was calculated according to the following equation and used for comparison of granule shape obtained from different screw configurations

$$VAR = d_a / h_{max} \quad (2)$$

where (d_a) is the equivalent diameter, and (h_{max}) is the maximum granule height. The (d_a) and the (h_{max}) were measured from the projected area view and the side view, respectively.

Results

Granulation in the conveying section

Figure 4A illustrates the size distribution of granules from the conveying section. The granules from this configuration have a characteristic bimodal size distribution. The first mode occurs between 63 and 90 μm , whereas the second mode is between 2 and 2.8 mm. With increasing L/S ratio, an increase

in the fraction between 2 and 2.8 mm is observed at the expense of that within 63 and 90 μm . Additionally, there is an increase in the fraction of granules above 2.8 mm in size. There is, however, very minimal change in the fraction of granules ranging from 125 to 710 μm . The first mode of the distribution corresponds to the size distribution of the raw blend.

The liquid distribution across the different size fractions is measured by virtue of the nigrosin dye dissolved in the granulating liquid. Figure 4B shows the mean concentrations of nigrosin ($n = 3$) at each size fraction, normalized to the weight of the granule sample, for L/S ratios of 0.15 and 0.2. A horizontal line independent of granule size indicates perfectly uniform liquid distribution. Figure 4B shows poor liquid distribution with the dye concentration highly dependent on the granule size. As the granule size increases, there is an incremental increase in the dye concentration, reaching a maximum at the largest size fraction for that experiment. Increasing the L/S ratio from 0.15 to 0.2, results in minimal difference in the dye concentration distribution across the different size fractions. The granule morphology obtained from

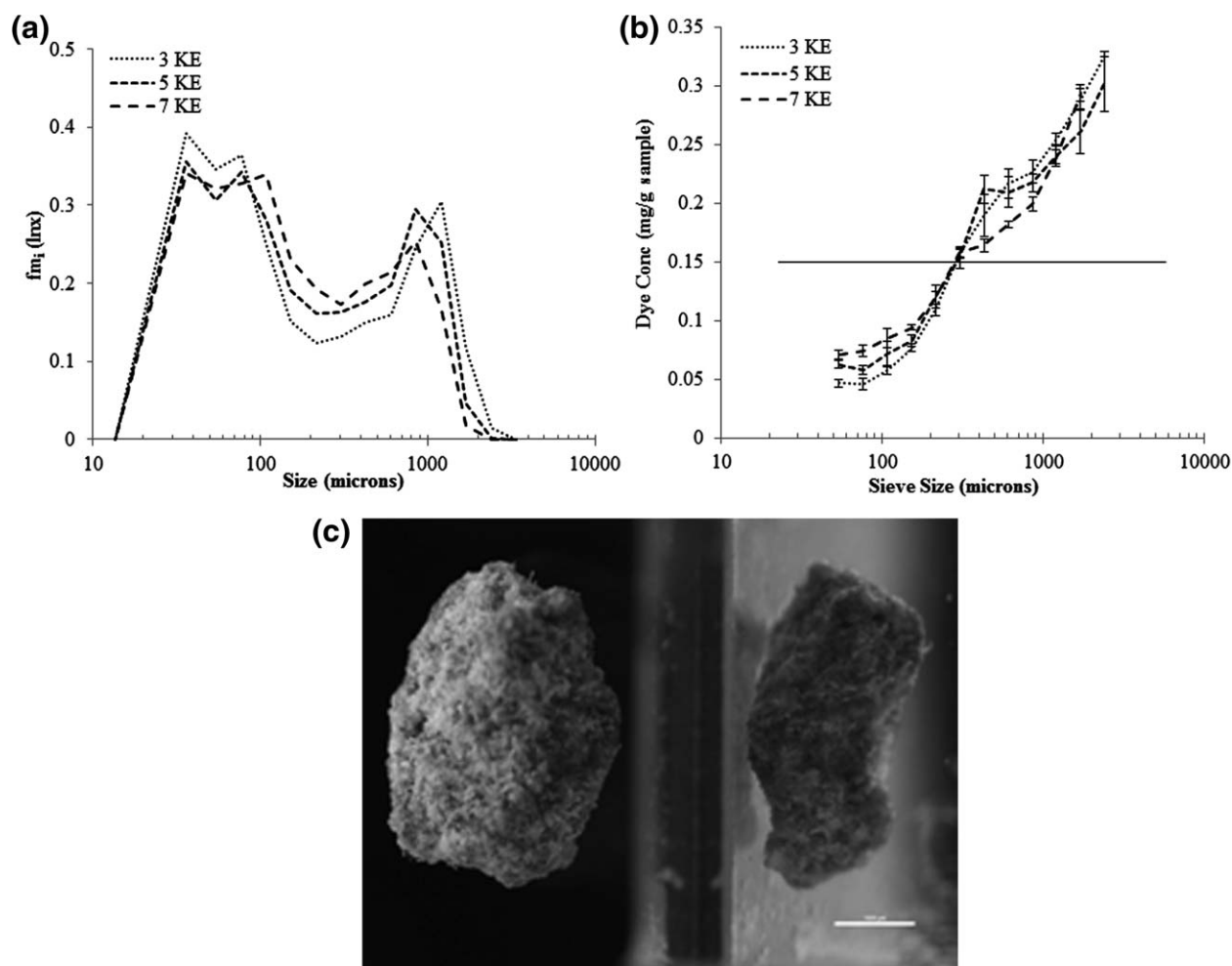


Figure 6. A. The frequency granule size distribution using 3 KE, 5 KE and 7 KE at 60°F angle configuration; B. dye distribution in granule size fractions using 3 KE, 5 KE and 7 KE at 60°F angle configuration; the horizontal solid line is the nominal dye concentration; the error bar at each data point is the standard deviation of three measurements; C. micrographs of top (left) and side (right) view of a representative granule from the 60°F kneading block configuration using 3 KE.

the conveying section is shown in Figure 4C. The left side of the image represents the top view of the granule and the right side shows the reflected height of the granule in the prism. The granule has an elongated shape, with a porous structure.

Granulation in the kneading section

As the granules travel from the conveying section into the kneading region of the granulator, the granule properties as well as the liquid distribution change. The kneading element results are first presented at a single L/S ratio of 0.15. The starkly different behavior for different kneading element configurations is shown most clearly at the low L/S ratio. For each configuration, we show the full size distribution and liquid distribution at three lengths of kneading blocks: 3KE, 5KE and 7 KE, as well as the granule morphology obtained from 3 KE. This level of data detail is necessary to understand the granulation rate processes. The effect of L/S ratio on granule growth in the different configurations is then presented, followed by quantitative 3-D granule shape characterization.

Effect of kneading block angle configuration and length

Figure 5A, 5B and 5C illustrate the size distribution, liquid distribution and typical granule morphology for the 30°F

kneading block configuration, respectively. The granule size distribution maintains the strong bimodal distribution from the conveying section shown in Figure 4B. As the number of KE increases, there is a decrease in fines, which shows as a decrease in the height of the first mode of the granule-size distribution. The reduction in fines corresponds to an increase in the frequency of granules in both the intermediate and large granule size range. Liquid distribution in the 30°F angle configuration is relatively poor as can be seen in Figure 5B, but does steadily improve as the number of KE is increased. Figure 5C shows granules that are similar in morphology to those from the conveying section.

Figure 6A shows the granule frequency size distribution for the 60°F kneading block configuration. The size distributions are very similar to those from the conveying section. Within experimental error, there is no effect of the number of KE on the granule size distribution. These results are consistent with the liquid distribution results shown in Figure 6B. The liquid distribution is poor with the 60°F kneading block configuration. There is very little difference from the conveying section, and minimal change as the number of KE is increased. Figure 6C shows a microscopic image of a typical granule obtained from the 60°F configuration, where the

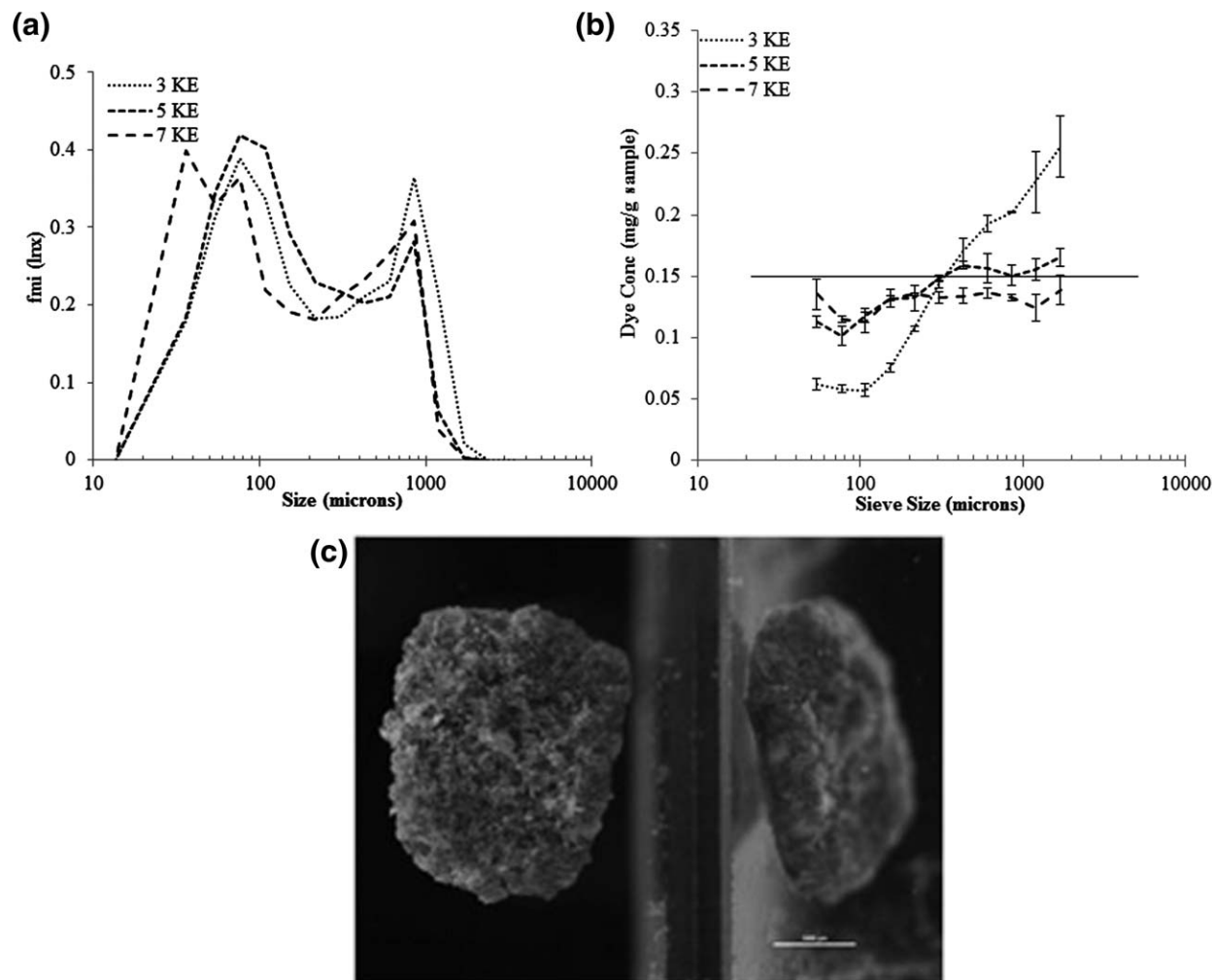


Figure 7. A. The frequency granule size distribution using 3 KE, 5 KE and 7 KE at 90° angle configuration; **B.** dye distribution in granule size fractions using 3 KE, 5 KE and 7 KE at 90° angle configuration; the horizontal solid line is the nominal dye concentration; the error bar at each data point is the standard deviation of three measurements; **C.** micrographs of top (left) and side (right) view of a representative granule from the 90° kneading block configuration using 3 KE.

granule morphology is similar to that from the conveying section.

Rotation of the advance angle to 90° increases the level of fines in the granule size distribution as illustrated in Figure 7A. The fraction of fines increases as more KE are added, where the size distribution profile of 7 KE is distinctly shifted to the left compared to 3 and 5 KE. The liquid distribution with 3 KE is poor, but displays considerable improvement with increasing the number of KE. The dye content of fines from 5 and 7 KE is higher than that from 3 KE, indicating that the fines generated from 5 and 7 KE originate primarily from breakage of granulated material. The granule morphology from the 90° configuration demonstrates a relatively rounder granule compared to the conveying section as can be seen in Figure 7C.

Figure 8A and 8B illustrate the size and liquid distribution of granules obtained from the 60°R configuration, respectively. The granule size distributions demonstrate less bimodal behavior at this L/S ratio. There is a more pronounced increase in the fraction of coarse granules and a corresponding reduction in the fraction of fines as more KE are added compared to the 60°F configuration in Figure 6A.

The liquid distribution (Figure 8B) demonstrates little dependence on the granule size even for the 3 KE. As the number of KE increases to 5 and 7, there is an increase in the homogeneity of liquid distribution. Two distinct populations of granule shapes are obtained with the 60°R kneading block configuration and are shown in Figure 8C and 8D. Figure 8C shows a rounded granule, similar to that obtained with the 90° angle configuration. Figure 8D displays a flatter granule shape. The granule is thin as seen from the reflected height to the right of the image.

Figure 9A illustrates a unique size distribution for the 30°R configuration that is similar for the three different kneading lengths used in the study. The granule size distribution from the 30°R configuration demonstrates a major mode of larger size granules, with a considerably diminished mode representing the fines as opposed to all other angle configurations at the same L/S ratio. The granule size distributions of 5 and 7 KE show a shift toward more coarse granules and a slightly reduced level of fines compared to that of 3 KE. Figure 9B displays the liquid distribution results for the 30°R configuration. The homogeneity of liquid distribution with the 30°R kneading block configuration is

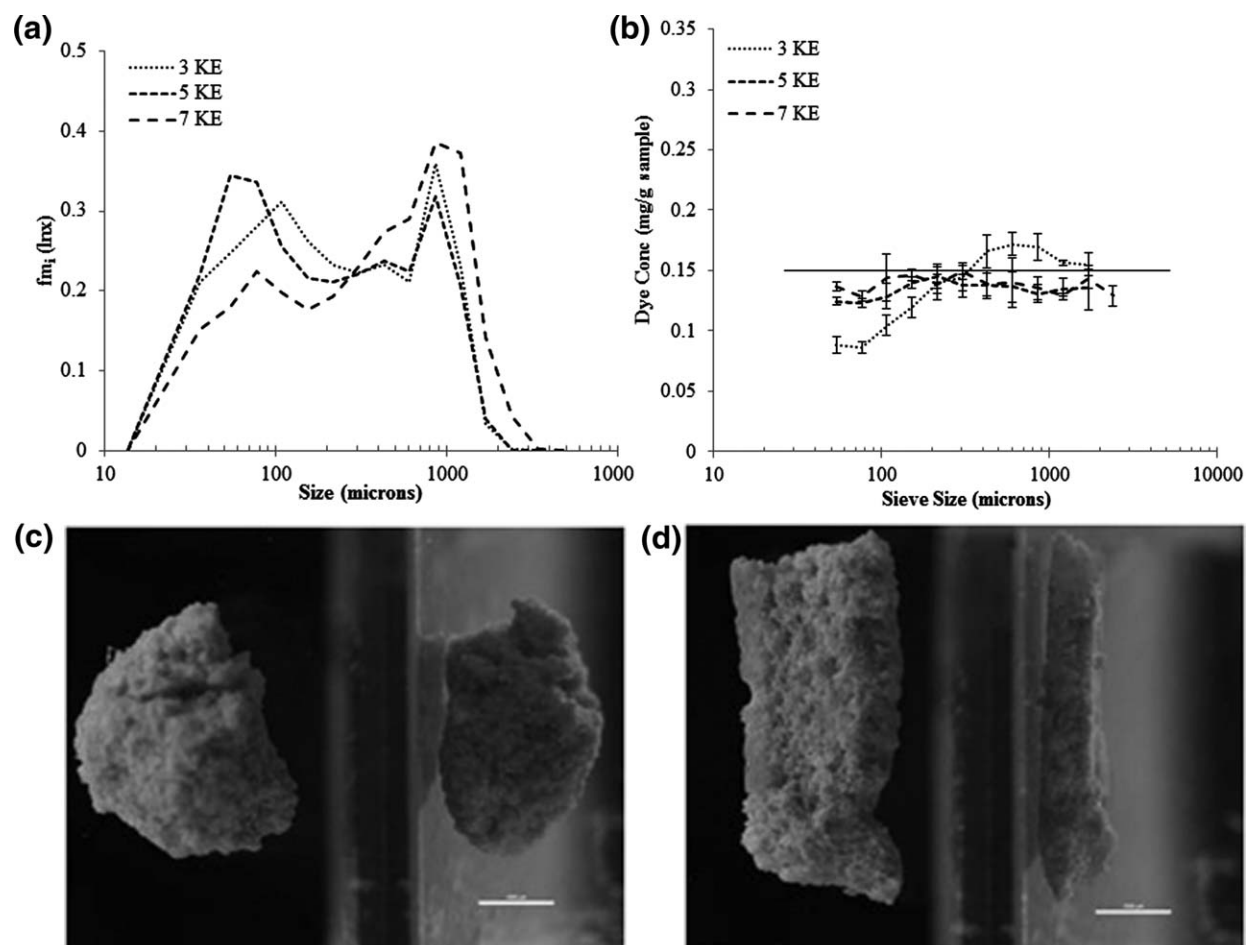


Figure 8. A. The frequency granule size distribution using 3 KE, 5 KE and 7 KE at 60°R angle configuration; B. dye distribution in granule size fractions using 3 KE, 5 KE and 7 KE at 60°R angle configuration; the horizontal solid line is the nominal dye concentration; the error bar at each data point is the standard deviation of three measurements; C. micrographs of top (left) and side (right) view of a representative rounded granule from the 60°R kneading block configuration using 3 KE; D. micrographs of top (left) and side (right) view of a representative flake-like granule from the 60°R kneading block configuration using 3 KE.

superior to all other configurations. The dye content is independent of granule size, especially for the 5 and 7 KE. Figure 9C displays a microscope image of a 30°R granule, showing a thin and flattened flake-like shape, with a bulge at the end. The granule shape is similar to that seen in some of the 60°R granules as represented in Figure 8D.

Table 2 summarizes the mean difference between the dye content in the largest and smallest granule size fraction for all configurations. For 3 KE, the homogeneity of liquid distribution follows the order 30°R > 60°R > 90° > 30°F > 60°F. With 5 KE, there is still a measurable variation among the different configurations that follows the same order as the 3 KE except for 30°R and 60°R configurations. In the reverse direction, both angles show the same effect on the dye distribution with 5 KE. The homogeneity of liquid distribution continues to improve with 7 KE for all configurations except for 60°F.

Effect of L/S ratio on granule growth

Figure 10A, 10B and 10C illustrate the effect of L/S ratio on the frequency granule size distributions of selected kneading block configurations: 3KE60°F, 3KE90° and 3KE30°R, respectively. The increase of L/S ratio produces a more monomodal granule size distribution for 60°F and 90° angle configurations

as a result of the loss of fines and progressive granule growth. The effect is more subtle with the 30°R configuration, which has a relatively more monomodal distribution at L/S ratio of 0.15 compared to 60°F and 90° kneading block configurations. However, further reduction in the level of fines and increase in the fraction of coarse granules is observed with the increase in L/S ratio. At L/S ratio of 0.35, the effect of kneading block configuration on granule size distribution is considerably diminished because of over-wetting. At this liquid content, a significant portion of the granules are larger than the maximum desired size.

The sensitivity of measured properties to L/S ratio can be further seen in Figure 11, which displays the %RSD of the dye content in all size fractions calculated across L/S ratios ranging from 0.15 to 0.45 using 3 KE60°R and 7 KE60°R. Increasing the L/S ratio from 0.15 to 0.45 reduces the variability in liquid distribution for the 3 KE from approximately 25 to 8%, respectively. Although the variability of liquid distribution for 7 KE shows little dependence on L/S ratio in this angle configuration, the difference in liquid distribution between the 3 and 7 KE is most pronounced at the lowest L/S ratio.

Figure 12 illustrates the granule growth with the increase of L/S ratio for all the offset angle configurations using 3, 5 and 7 KE. With 3 KE, the reverse angle configuration

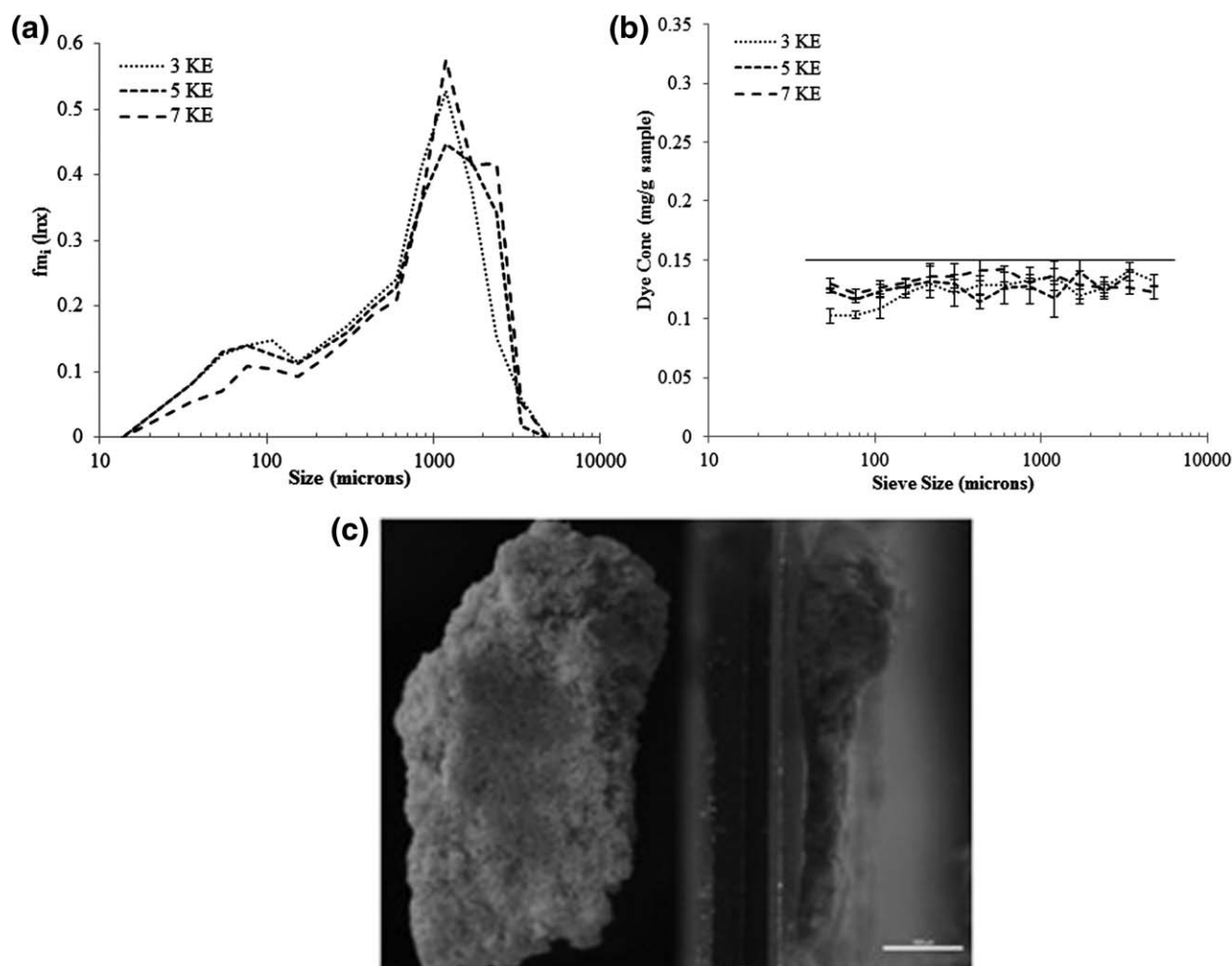


Figure 9. A. The frequency granule size distribution using 3 KE, 5 KE and 7 KE at 30°R angle configuration; B. dye distribution in granule size fractions using 3 KE, 5 KE and 7 KE at 30°R angle configuration; the error bar at each data point is the standard deviation of three measurements; C. micrographs of top (left) and side (right) view of a representative granule from the 30°R kneading block configuration using 3 KE; the horizontal solid line is the nominal dye concentration.

considerably increases the granule size for both 30° and 60° angles compared to the forward angle across the range of L/S ratios used in the study (Figure 12A). The 90° angle follows an intermediate path between the reverse and the forward angles. A similar effect can be seen in Figure 12B for 5 KE. The effect of angle direction, however, is less distinct with 7 KE, especially with the increase in L/S ratio. The difference in d_{50} between each angle in its forward and reverse directions diminishes beyond L/S ratio of 0.2. At the lower L/S ratios, the 30° angle in both the forward and reverse directions results in larger d_{50} values compared to 60°, regardless of the length of the kneading section. The granule size for forward angle configurations does not show a significant increase in the number of KE from 3 to 5 to 7. However, the extent of granule growth in the kneading section with 7 KE at 90°, 30°R and 60°R is less compared to that obtained from 3 or 5 KE, especially with the increase in L/S ratios beyond 0.2.

Quantitative granule shape characterization

The difference in granule morphology among the different screw configurations is evaluated using the vertical aspect ratio (VAR). The side view of most 30°R and some 60°R

granules shows a bulge at one end as can be seen in Figure 9C, which overestimates the height of the granule if this part is used. So, this portion is excluded from the calculation of the height and an average of three height measurements along the length of the rest of the granule is used instead. The same approach is used for measuring the height of any granules demonstrating the same morphology. Figures 4C–9C show that the images from the reverse angle

Table 2. Difference in Dye Content between largest and Smallest Granule Size Fraction for Different Screw Configurations at L/S Ratio = 0.15.

Configuration	Mean \pm St.dev. (mg/g)		
	3 KE	5 KE	7 KE
30°F	0.27 \pm 0.005	0.17 \pm 0.014	0.01 \pm 0.009
30°R	0.03 \pm 0.010	0.01 \pm 0.010	— ^a
60°F	0.28 \pm 0.006	0.24 \pm 0.027	0.22 \pm 0.010
60°R	0.07 \pm 0.016	0.01 \pm 0.010	— ^a
90°	0.19 \pm 0.021	0.05 \pm 0.009	0.003 \pm 0.004
Conveying		0.39 \pm 0.012	

^anegative values

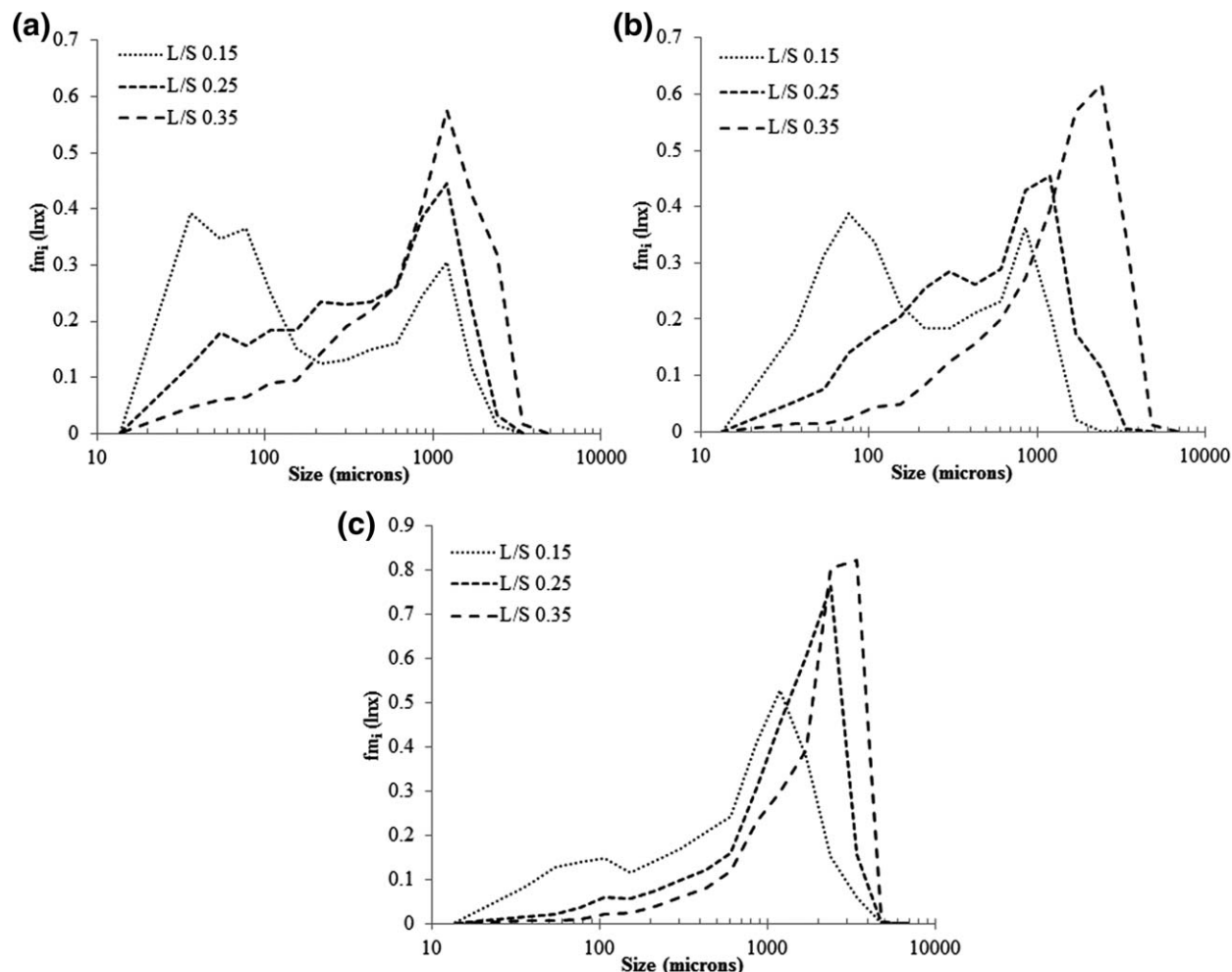


Figure 10. Frequency granule size distributions at L/S ratios of 0.15, 0.25 and 0.35 using (A) 3KE60°F, (B) 3KE90° and (C) 3KE30°R.

configurations are flattened and thinner than those from the CE or the neutral angle configuration.

Figure 13 illustrates the distribution of VARs for the CE and all configurations of 3 KE. There is a distinct difference in the 3-D granule shape distribution between the 30°R and 60°R configurations on one hand and the rest of the configurations. The 30°R and 60°R configurations have an overall larger VAR, with a considerably wider distribution of granule shapes compared to the forward, neutral and CE configurations. The 60°R configuration displays a bimodal distribution of VARs of granules with the larger mode resembling the 30°R pattern whereas the smaller mode resembles those from all the other configurations. The first and second modes correspond to the granules depicted in Figure 8C and 8D, respectively.

Discussion

Proposed granulation rate processes

Table 3 summarizes the dominant granulation rate processes for the conveying and kneading sections of a TSG. The proposed rate processes are based on the 3-D information obtained from size, shape and liquid distribution characterization in each configuration. There is a dominant mechanism(s) by which liquid distribution and granule shape formation take place in each kneading section configuration.

These two attributes of the granular product give rise to size properties and growth behavior that are unique to each particular configuration.

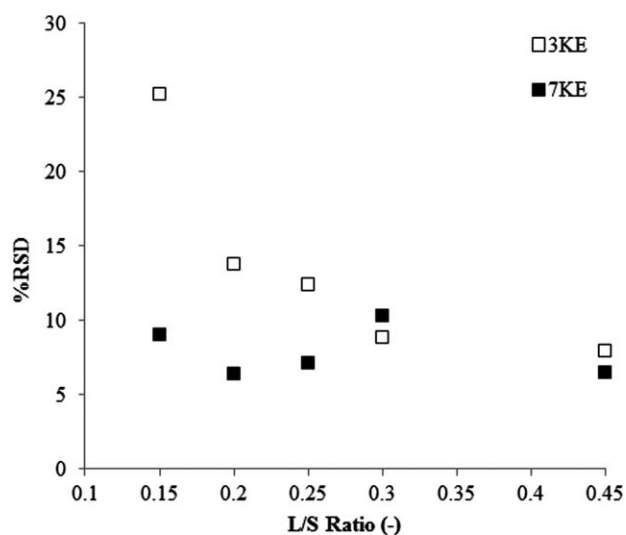


Figure 11. % RSD of dye distribution across all size fractions as a function of L/S ratio using 3KE60°R and 7KE60°R.

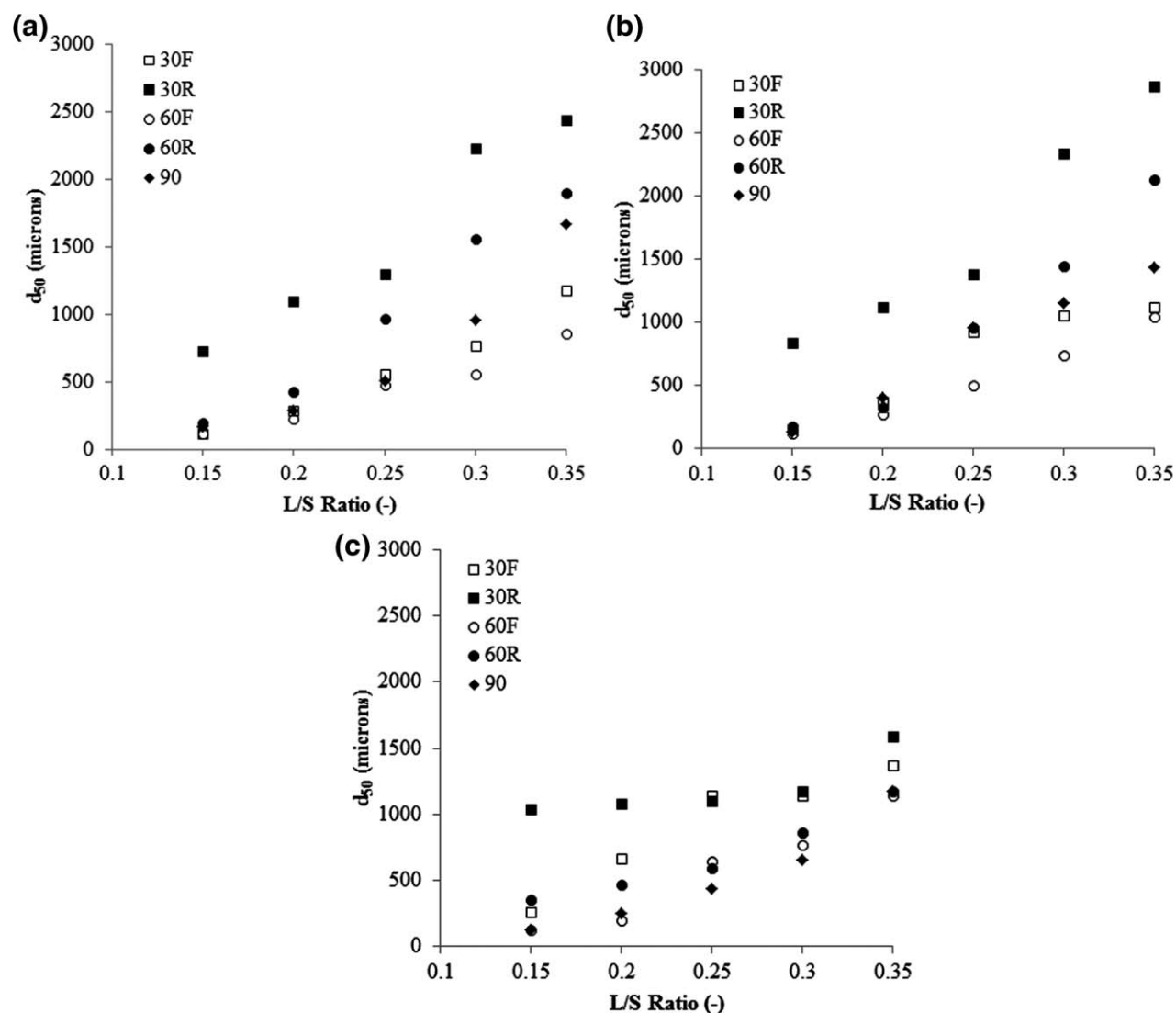


Figure 12. Granule growth as a function of L/S ratio using different angle configurations of (A) 3 KE, (B) 5 KE and (C) 7 KE.

In the conveying section, agglomerates are formed by drop-granulation as the liquid is dripped into the barrel producing bimodal size distribution of ungranulated fines and wet agglomerates (Figure 4A). The wet agglomerates pick up fines from the surrounding powder through a layering mechanism. At high L/S ratios, more wet agglomerates are formed and the likelihood of droplet coalescence increases. So, the fraction of coarse granules increases at the expense of the fines as seen in Figure 4A. Minimal liquid distribution and shape transformation occurs in this section, regardless of the L/S ratio used (Figure 4B and 4C).

The wet agglomerates emerging from the conveying section are subjected to different breakage and consolidation events in the kneading section, depending on the exact screw configuration as shown in Table 3. The two main rate processes by which the granule shape, size and liquid distribution evolve can be summarized by:

1. Breakage, followed by layering; and
2. Shear-elongation and breakage, followed by layering.

The 90° and 30°R configurations represent the two extremes of the proposed mechanisms and are, thus, described first.

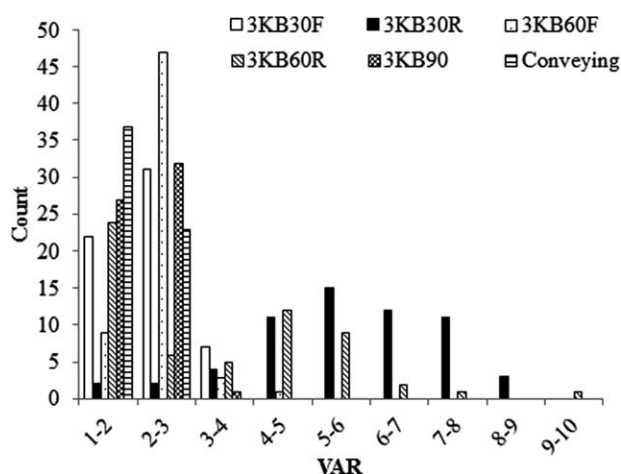


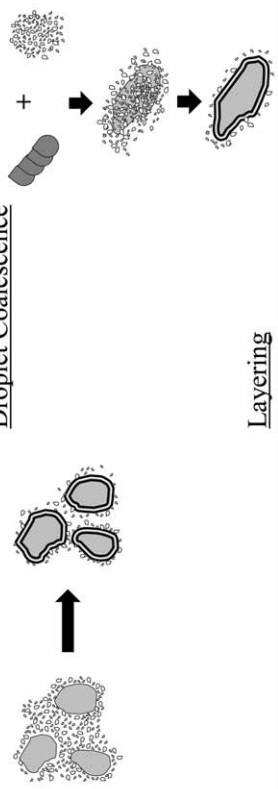
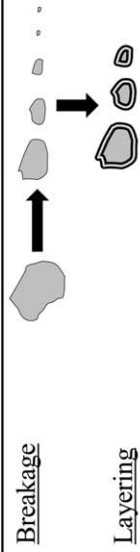

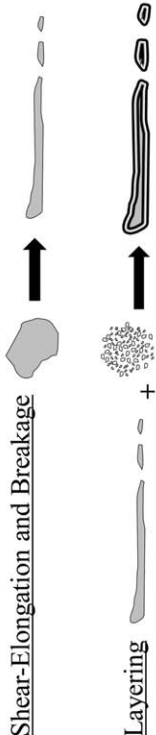

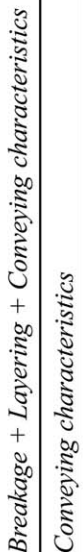



Figure 13. The distribution of VAR for granules ($n = 60$) from different screw configurations in the size range from 2.0–2.8 mm.

Table 3. Proposed Granulation Rate Processes in a Twin Screw Granulator

Screw Type	Dominant Rate Processes	More KE	
		Liquid Distribution	Granule Growth
	Drop Nucleation (DN)		NA
	Layering		NA
	Conveying		NA
Neutral	Breakage		-
Reverse	Layering		+
	30°		+
	60°		+
Forward	30°		+
	60°		Nil
NA: Not applicable		+ Positive Change	- Negative Change
		Nil: No Change	

The KE in the neutral 90° configuration intersect in the middle channel more frequently than any other possible configuration in the kneading section (Figure 2E). The rotating tips of the KE chop-off the edges of wet agglomerates arising from the conveying section, forming rounded granules (Figure 7C) that can grow by layering. The newly exposed wet surface of the fragments picks up dry fines by layering. The layering mechanism improves the liquid distribution compared to CE only. The addition of more KE subjects the wet agglomerates to more breakage events, leading to an increase in the level of generated fines and a reduction of granule mean size as shown in Figure 7A. However, the liquid distribution improves with longer kneading sections because of the additional exchange of granulating liquid between the wet surface of chopped consolidated granules and the ungranulated fines along the axial direction of material flow as shown in Figure 7B.

In the 30°R configuration, the KE are staggered such that the middle channel gap extends over 1.25D in the axial direction (Figure 2B). In the reverse configuration, the main passage for the material from CE is through smearing against the barrel wall, leading to shear-elongation of the wet agglomerates. In addition to flattening the rounded agglomerates into flakes as depicted in Figure 9C, consolidation and squeezing the water to the surface occurs, which provides a large, freshly wet surface area for particle layering to take place. Note that the flake-like particles appear “larger” in sieve size analysis due to their change in shape, rather than an increase in volume. The excessive thinning of the granules, as a result of smearing, leads to breakage and formation of smaller fragments that can act as substrates for fines’ layering as well. The increase in the number of KE results in smearing of a progressively larger number of wet agglomerates from the conveying section. Thus, more surfaces become available for layering, which ultimately decreases the level of fines, results in more granule growth and improves the liquid distribution as can be seen in Figure 9A and 9B, respectively.

In the 60°R kneading block configuration shown in Figure 2D, the tips of the KE are neither closely staggered against the barrel wall nor alternating between the barrel wall and the middle channel as in case of the 30°R and 90° configurations, respectively. Thus the 60°R configuration gives a combined mechanism that is more subtle than either extreme. The distribution of VARs of granules strongly reflects that mixed mechanism in the 60°R configuration, where the distribution of shapes combines features from both the 30°R and the 90° configurations as illustrated in Figure 13. Furthermore, the size distributions of 60°R in Figure 8A demonstrate an incremental increase in the level of fines for each set of KE compared to their 30°R counterparts shown in Figure 9A. In addition, there is a decrease in the homogeneity of liquid distribution for 3 KE with the increase in the angle from 30°R to 60°R as seen in Table 2. The addition of more KE in the 60°R configuration accentuates the smearing mechanisms, thereby improving the liquid distribution and increasing granule growth.

The orientation of the KE in the 30°F configuration provides a path for the material to flow forward along the middle channel rather than being smeared along the barrel wall. So, the granulation mechanism in the 30°F configuration is similar to that in the 90° angle configuration, albeit with less breakage and possibly less consolidation. As a result, the liquid distribution in case of the 30°F is worse compared to

90°. The addition of more KE provides longer time for breakage and consolidation events to take place, resulting in improved liquid distribution (Figure 5B) and more granule growth (Figure 5A).

The most interesting observation from the analysis of granule size and liquid distribution data is that the 60°F configuration provides the worst liquid distribution even with the use of 7 KE. The 60°F configuration provides a smooth passage through the center channel, while avoiding smearing and chopping as seen with the 30° and 90° configurations, respectively. In addition, the 60°F is expected to have a shorter residence time relative to other configurations,²⁶ leading to less material holdup and back-mixing, which negatively affects the granulation efficiency even more. Unlike other configurations, the addition of more KE does not improve the inherent poor mixing attributes characteristic of the 60°F configuration. In fact, the physical properties of granules obtained from this are analogous to an equivalent length of CE with limited liquid distribution and hence granulation capabilities. Although liquid distribution and granule growth change slightly in the 60°F configuration compared to just CE, the difference probably occurs at the transition of the wet agglomerates from the conveying into the kneading section, without any further change even with the addition of more KE.

The granule growth data presented in Figure 12A–C support the proposed granulation rate processes. The reverse angle configurations display a higher extent of growth as a function of L/S ratios in comparison to the forward angle configurations in case of 3 and 5 KE. The improved liquid distribution in the reverse angle makes the granulating liquid more available for granulating the fine particles, thereby increasing the granule growth. The reduced d_{50} observed for 60°R and 90° angle configurations as the number of KE increased to 7 can be attributed to increased breakage. For the neutral angle configuration, the breakage is primarily occurring in the middle channel from squeezing the material between the rotating kneading tips, whereas for the 60°R, it is a balance between smearing the granules against the barrel wall and the chopping mechanism between the kneading tips in the middle channel.

The shape characterization results in Figure 13 further support the proposed rate processes. The smearing of agglomerates in the 30°R angle configuration produces granules with a broad distribution of VAR values. In contrast, the forward and neutral angle configurations as well as the CE have an overall similar distribution of VARs, which is narrow and shifted to the left. The significantly lower VARs in this case can be attributed to less smearing, where the material moving forward has an alternative path in the middle channel as opposed to being smeared against the barrel wall. In the middle channel, the wet agglomerates are rounded off by chopping their edges, thereby producing a lower VAR. The 60°R VAR histogram displays a bimodal distribution with the larger mode resembling the 30°R pattern whereas the smaller mode resembles those from all the other configurations, indicating the overlap of granulation mechanisms in this particular configuration, which is intermediate between the two extreme cases of 30°R and 90°.

Thompson et al. reported the occurrence of qualitatively distinct granule shapes, depending on the screw configuration used.¹⁰ However, the 2-D shape factor used in their study does not fully distinguish the granule shapes obtained with the different screw configurations. Indeed, the data obtained from the 2-D shape characterization in this study does not reveal the difference in granule shapes. In contrast,

incorporation of the third dimension of the granule into the shape parameter through the use of the VAR provides a clear distinction of granule shape, depending on the dominant granulation mechanism(s) in a particular configuration. The overall distribution of shapes illustrated in Figure 13 indicates that besides the dominant granulating rate processes in a particular configuration, a distribution of other less significant mechanisms takes place as well.

The conveying section in twin screw granulators

The characteristics of agglomerates formed in the conveying section agree with the results reported by Dhenge et al. in which the granulation is carried out in the conveying section compartment only.^{12,14} The authors report the formation of loosely aggregated large agglomerates due to the addition of granulating liquid in a dripping mode, similar to the granule morphology depicted in Figure 4C. The abundance of channels in the conveying section creates regions that are significantly less shear-intensive compared to other mixing regions in the granulator.²⁷ The combined effect of relatively large-size liquid droplets, with respect to the particle size, as well as the absence of shearing force results in nucleation by immersion rather than distribution mechanism.²⁸

With the low-shear environment in the conveying section, the liquid droplets from the nozzle are not subjected to mixing with the rest of the powder particles in the barrel, resulting in poor liquid distribution. The addition of more granulating liquid does not change the liquid distribution profile in the conveying section as seen in Figure 4B. Regardless of the L/S ratio used, visual examination of granules at or above 710 microns demonstrates a color gradient across their surface, indicating layering of fine particles. The micrograph in Figure 4C shows the presence of a color gradient across the granule surface. The layering mechanism is facilitated by the wet surface of these granules as they are transported along the conveying section.

Comparison with kneading elements' characterization in extrusion systems

The extrusion literature provides considerable analysis of the flow fields associated with twin screw elements, which is valuable in understanding granulation mechanisms in a TSG. There are different mass-transfer regions in a twin screw system according to the location of the material with respect to a specific area on the kneading element.²⁷ For co-rotating twin screw systems, the tips and lobes of a kneading element provide the strongest shear mixing effects. The latter regions are also characterized by strong extensional mixing action. The characteristics of KE described in the extrusion literature strongly support our observations with the TSG. The KE in the 30°R configuration squeeze the large wet agglomerates from the conveying section along the barrel wall by virtue of the close staggering of their tips in that direction. The wet material is captured to a greater extent in the lobal pool of the KE, thereby exposing it to more shear-elongation and smearing.

Previous work in the extrusions literature has also demonstrated that the different angle configurations for a given set of KE impart significantly different mixing and conveying abilities.^{26,29,30} It has been shown that KE with smaller offset angles in the forward direction have improved conveying capabilities over larger forward angles or reverse angles. According to Bravo et al. a pseudo-helix angle that is derived from the advance angle and width of the discs

defines the channel discontinuities in kneading sections of different configurations.²⁹ The pseudo-helix angle modifies the conveying properties of KE by changing the size of the backflow region on the advancing disks that hinders the axial flow of the material. As a result, the residence time distribution of small forward angles is characterized by long tails due to more spreading in the axial direction of the equipment compared to large forward or reverse angles.²⁶ However, the axial spreading occurs at the expense of mixing with the surrounding particles, leading to "pipeline flows" and poor mixing behavior. The tracer studies conducted to evaluate the mixing and conveying properties of KE at 30°F, 60°F, 90°, 60°R and 30°R configurations demonstrate that the 60°F has the widest axial spread of the tracer used, indicating the best conveying and the worst mixing behavior among all other angle configurations. The effect of angle direction on growth of the interfacial area of the tracer shows that the rate of interfacial growth is faster with the reverse angle because of more prominent reorientation of interfacial areas, leading to superior mixing characteristics over forward angles.

The findings from the studies on flow characterization inside twin screw extruders strongly support our own results regarding granule formation mechanisms in relation to liquid distribution characteristics inside a TSG. In contrast to the different degrees of channel fill that are possible with the conveying section in a TSG, the kneading section operates completely full with material.¹⁰ So, in this respect the mixing behavior as a function of kneading element configuration in a TSG bears some resemblance to that in an extrusion process.

Implications of granule attributes for downstream processing and mathematical modeling

The multidimensional information from size, shape and liquid distribution analyses clearly shows the interplay of multiple granulation rate processes inside a twin screw granulation process including drop nucleation, layering, shear-elongation and breakage. Except for shear-elongation, all other described rate processes have been reported previously for other conventional types of granulators. The shear-induced elongation and breakage of granules has been studied by Khan and Tardos in an idealized shear flow field using a fluidized Couette device.³¹ However, the special design of the KE and the confined granulation space give rise to this unique smearing mechanism in a TSG. It is this mechanism that results in the optimum liquid distribution characteristics for this process as seen with the 30°R configuration. However, the liquid distribution is just one aspect of a whole spectrum of granule properties that need to be optimized. The flake-like granule shape obtained with the 30°R configuration is not desirable from a manufacturing perspective due to possible handling problems during downstream processing such as friability and flowability. Granule porosity is another critical granule attribute because of its impact on downstream processes such as tablet compression. Although porosity is not evaluated in this study, it will undoubtedly be influenced by the different configurations of the kneading section. It is clear that optimization of screw configuration for producing custom-designed granule properties is not a straightforward process and will need to take into consideration all those factors combined. However, understanding the granulation rate processes governing the

evolution of granule properties in the individual screw elements serves as the basis for achieving this goal.

The bimodal size distribution characteristic of the twin screw granulation process is now proven experimentally to reflect liquid distribution inhomogeneity and/or breakage events characteristic of particular configurations. Our results show that the liquid distribution and granule shape attributes significantly affect the size distribution and granule growth behavior. Prediction of granule growth behavior requires the development of models that can take into account the effect of granule properties on granulation rate processes.²³ A 1-D population balance model (PBM), in which the granule size is assumed to be the only important attribute, will significantly limit the model's predictive capability in case of a twin screw granulator because of the heterogeneity of granule shape and liquid distribution. A multidimensional PBM that incorporates the effect of varying granule attributes is thus a more reasonable approach. Mechanistic understanding of the functional role of individual screw elements through characterization of different granule attributes provides a comprehensive framework for the development of a multidimensional PBM of this process that can be implemented for future process optimization and control.

Conclusions

In this mechanistic study, characterization of individual screw elements in a TSG was carried out through analyzing the physical and liquid distribution attributes of the granules obtained from each screw configuration type. The kneading section configuration significantly affected the granule shape and liquid distribution efficiency, which in turn determined the resulting granule size distribution. The two main rate processes occurring in the kneading section of a TSG were:

1. Breakage, followed by layering.
2. Shear-elongation and breakage, followed by layering.

The aforementioned extreme granulation mechanisms were dominant in the 90° and 30°R configurations, respectively. The other configurations demonstrated some combination thereof to varying degrees of intensity. The liquid distribution efficiency for the different angle configurations using 3 KE could be ranked in the following order from best to worst: 30°R > 60°R > 90° > 30°F > 60°F. The 60°F demonstrated similar attributes to an equivalent length of conveying elements, rendering it the worst choice in attempting to achieve superior mixing performance even with the addition of more KE.

The 3-D information obtained from size, shape and liquid distribution were indispensable in identifying the granulation processes for the conveying and kneading elements and explaining the broad granule size distribution characteristic of a twin screw granulation process. The results show that no combination of KE can completely recover from the effects of poor liquid distribution in the dripping mode in the initial conveying element section, without dramatically changing other granule attributes.

Acknowledgements

This work is supported by the Engineering Research Center for Structured Organic Particulate Systems through a grant from the National Science Foundation for Commercialization Project (Grant no. 0951845). The authors thank GlaxoSmithkline for the kind donation of raw materials and a

gravimetric powder feeder. Professor Lisa Mauer is acknowledged for granting access to the centrifuge used in the study, Steven Dale for providing the schematics of kneading block configurations, and Ming Tay for assistance with the shape characterization.

Literature Cited

1. Ennis JB, Litster JD. Particle Size Enlargement. In: Perry R, Green D, eds. *Perry's Chemical Engineers' Handbook*. New York: McGraw-Hill 1997:20–56.
2. Leuenberger H. New trends in the production of pharmaceutical granules: batch versus continuous processing. *Euro J Pharm Biopharm*. 2001;52:289–296.
3. Plumb K. Continuous processing in the pharmaceutical industry. Changing the mind set. *Chem Eng Res Des*. 2005;83:730–738.
4. Vervaet C, Remon JP. Continuous granulation in the pharmaceutical industry. *Chem Eng Sci*. 2005;60:3949–3957.
5. Djuric D, Kleinebudde P. Continuous granulation with a twin-screw extruder: Impact of material throughput. *Pharm Dev Technol*. 2010;15:518–525.
6. Djuric D, Kleinebudde P. Impact of screw elements on continuous granulation with a twin screw extruder. *J Pharm Sci*. 2008;97:4934–4942.
7. Keleb EI, Vermiere A, Vervaet C, Remon JP. Twin screw granulation as a simple and efficient tool for continuous wet granulation. *Int J Pharm*. 2004;273:183–194.
8. Melkebeke BV, Vervaet C, Remon JP. Validation of a continuous granulation process using a twin-screw extruder. *Int J Pharm*. 2008;356:224–230.
9. Shah U. Use of a modified twin-screw extruder to develop a high strength tablet dosage form. *Pharm Technol*. 2005;29:52–66.
10. Thompson MR, Sun J. Wet granulation in a twin screw extruder: implications of screw design. *J Pharm Sci*. 2010;99:2090–2103.
11. El Hagras A, Hennenkamp J, Burke M, Cartwright J, Litster J. Twin screw wet granulation: influence of formulation parameters on granule properties and growth behavior. *Powder Technol*. 2012;238:108–115.
12. Dhenge RM, Cartwright JJ, Hounslow MJ, Salman AD. Twin screw granulation: Steps in granule growth. *Int J Pharm*. 2012;438:20–32.
13. Dhenge RM, Cartwright JJ, Hounslow MJ, Salman AD. Twin screw wet granulation: Effects of properties of granulation liquid. *Powder Technol*. 2012;229:126–136.
14. Dhenge RM, Washino K, Cartwright JJ, Hounslow MJ, Salman AD. Twin screw granulation using conveying screws: Effects of viscosity of granulation liquids and flow of powders. *Powder Technol*. 2012;238:77–90.
15. Michaels JN, Farber L, Wong GS, et al. Steady states in granulation of pharmaceutical powders with application to scale-up. *Powder Technol*. 2009;189:295–303.
16. Dhenge RM, Fyles RS, Cartwright JJ, Doughty DG, Hounslow MJ, Salman A. Twin screw granulation: Granule properties. *Chem Eng J*. 2010;164:322–329.
17. Djuric D, Melkebeke BV, Kleinebudde P, Remon JP, Vervaet C. Comparison of two twin-screw extruders for continuous granulation. *Eur J Pharm. Biopharm*. 2009;71:155–160.
18. Ax K, Feise H, Sochon R, Hounslow M, Salman A. Influence of liquid binder dispersion on agglomeration in an intensive mixer. *Powder Technol*. 2008;179(3):190–194.
19. Knight P, Instone T, Pearson J, Hounslow M. An investigation into the kinetics of liquid distribution and growth in high shear mixer agglomeration. *Powder Technol*. 1998;97(3):246–257.
20. Reynolds G, Biggs C, Salman A, Hounslow M. Non-uniformity of binder distribution in high-shear granulation. *Powder Technol*. 2004;140(3):203–208.
21. Smirani-Khayati N, Falk V, Bardin-Monnier N, Marchal-Heussler L. Binder liquid distribution during granulation process and its relationship to granule size distribution. *Powder Technol*. 2009;195(2):105–112.
22. Wauters PAL, Jakobsen RB, Litster JD, Meesters GMH, Scarlett B. Liquid distribution as a means to describing the granule growth mechanism. *Powder Technol*. 2002;123(2):166–177.
23. Iveson SM. Limitations of one-dimensional population balance models of wet granulation processes. *Powder Technol*. 2002;124(3):219–229.
24. Allen T. *Powder Sampling and Particle Size Determination*. 1st ed. Amsterdam, The Netherlands: Elsevier; 2003.

25. Emady HN, Kayrak-Talay D, Schwerin WC, Litster JD. Granule formation mechanisms and morphology from single drop impact on powder beds. *Powder Technol.* 2011;212:69–79.
26. Kalyon DM, Sangani HN. An experimental study of distributive mixing in fully intermeshing, co-rotating twin screw extruders. *Polym Eng Sci.* 1989;29(15):1018–1026.
27. Thiele W. Twin Screw Extrusion and Screw Design. In: Ghebre-Sellasie I, Martin C, eds. *Pharmaceutical Extrusion Technology*. New York: Marcel Dekker, Inc.; 2003:69–98.
28. Schæfer T, Mathiesen C. Melt pelletization in a high shear mixer. VIII. Effects of binder viscosity. *Int J Pharm.* 1996;139(1):125–138.
29. Bravo V, Hrymak A, Wright J. Study of particle trajectories, residence times and flow behavior in kneading discs of intermeshing co-rotating twin-screw extruders. *Polym Eng Sci.* 2004;44(4):779–793.
30. Lawal A, Kalyon DM. Mechanisms of mixing in single and co-rotating twin screw extruders. *Polym Eng Sci.* 1995;35(17):1325–1338.
31. Khan MI, Tardos GI. Stability of wet agglomerates in granular shear flows. *J Fluid Mech.* 1997;347:347–368.

Manuscript received Dec. 3, 2012, revision received Apr. 19, 2013, and final revision received Jun. 21, 2013.